Effect of mechanical and thermo-mechanical treatments on fatigue behaviour of V-shaped notched round bars

Andrea Carpinteri, Roberto Brighenti, Sabrina Vantadori

Department of Civil and Environmental Engineering & Architecture, University of Parma, Italy
E-mail: andrea.carpinteri@unipr.it

Keywords: notched bar, residual stresses, fatigue.

SUMMARY. In the present paper, the fatigue behaviour of a metallic round bar with a V-shaped circumferential notch and a surface crack at the notch root is examined. The bar is subjected to pulsating tension, and different crack shapes are considered: almond, sickle, straight-front crack. Residual stresses due to the cold-drawing process are herein considered and, since they are detrimental to fatigue life, two treatments are devised in order to decrease them, more precisely: (1) a further drawing with a very small area reduction (about 1%); (2) a procedure based on a combination of heating and stretching of the bar. The strong dependence of the fatigue crack propagation on the residual stress field is quantified in terms of evolution of both surface crack shape and crack growth rate.

1 INTRODUCTION

Eigenstresses, for example residual stresses, are defined as the stresses inside a component or structure after all applied loads have been removed, that is, the stresses without external loads applied [1]. Residual stresses are generated, upon equilibrium of material, after inhomogeneous plastic deformations are caused by mechanical, thermic or chemical phenomena during manufacturing and processing. In absence of external loads, the residual stress distribution must satisfy equilibrium, and therefore both tensile and compressive residual stresses arise.

Under the linear elastic material behavior hypothesis, the total stress field experienced by the material is equal to the residual stresses added to the stresses caused by the external load. If fatigue load is applied, the residual stresses modify only the mean value of the cyclic load, not the stress amplitude. In particular, a tensile residual stress increases the mean value and may produce a detrimental effect on fatigue behavior, while a compressive residual stress reduces the mean value and may significantly improve the fatigue resistance.

In the present paper, the residual stresses due to cold-drawing process and post-drawing treatments (mechanical and thermo- mechanical) are considered. More precisely, the effect of such stresses on the fatigue behavior of a metallic round bar with a V-shaped circumferential notch and an elliptical-arc surface crack at the notch root (Fig. 1) is analysed. The bar is subjected to pulsating tension. Several authors have numerically and experimentally examined the behavior of notched bars under different fatigue loading conditions without taking into account the effect of residual stresses [2-5], and only a few studies have discussed the influence of the residual stresses [6-8].

Different crack shapes are hereafter considered: almond, sickle, straight-front crack (the last one being the limit case between the two first types). Such shapes are as those experimentally observed (Ref.[9]).

The stress intensity factor (SIF) along the crack front due to the axial loading and residual stresses is computed by employing a three-dimensional finite element model, the power series expansion

of the residual stress field and the superposition principle. Then, by employing the SIFs evaluated, the fatigue crack propagation is modelled by means of a modified Paris-Erdogan law [10, 11]. The effect of the cold-drawing process and post drawing treatments on the fatigue life of the bar is examined for some initial configurations of the surface crack.

2 PROBLEM EXAMINED

The structural component being examined is a round bar with a V-shaped circumferential notch characterized by a depth c, an opening angle γ, a constant notch root radius ρ (Fig. 1). The diameter of the bar is equal to D_0 in an unnotched cross-section and equal to D in the reduced cross-section S-S (Fig. 1). The relative notch depth $\delta = c / D_0$ and the dimensionless notch root radius $\rho_d = \rho / D_0$ are assumed to be equal to 0.2 (i.e. D = 0.6 D_0) and 0.009, respectively, whereas the opening angle γ is equal to $60°$.

A surface crack with an elliptical-arc shape is assumed to exist at the notch root (Fig. 2). Three different crack shapes are considered: sickle crack (also called crescent-moon crack) (Fig. 2a), almond crack (Fig. 2b), and straight crack (which is the limit case between the first two types).

The crack configuration is described by two parameters: ξ and α. The relative crack depth $\xi = a / D$ of the most internal point A on the defect front (Fig. 2) is made to vary from 0.1 to 0.8. The crack aspect ratio $\alpha = a_{el} / b_{el}$, where a_{el} and b_{el} are the semi-axes of the ellipse describing the crack front, ranges from 0.0 to −1.2 for sickle-shaped cracks (Fig. 2a) and from 0.0 to 1.2 for almond-shaped cracks (Fig. 2b), whereas the straight-fronted crack is represented by $\alpha = 0.0$. The generic point P along the crack front is identified by the dimensionless coordinate $\zeta^* = \zeta / h$ (Fig. 2).

Firstly, residual stresses due to cold-drawing process, consisting of pulling the lubricated bar through a die thus reducing its cross-sectional area and increasing its length, are considered [6]. Then, residual stress distributions due to two post drawing treatments are examined: (1) a further drawing with a very small area reduction (about 1%); (2) a combination of heating (at 400°C) and stretching [6].

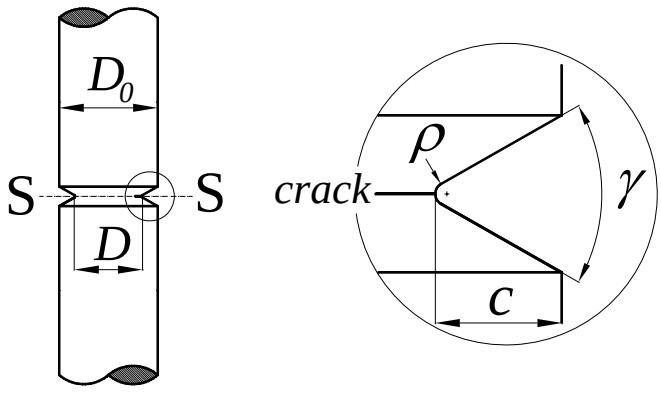

Figure 1: Geometrical parameters of the V-shaped circumferential notch in a round bar.

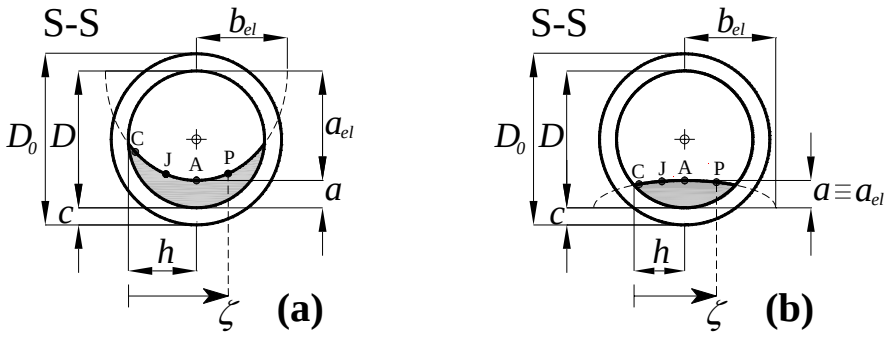

Figure 2: Geometrical parameters: (a) sickle -shaped surface crack; (b) almond -shaped surface crack.

3 RESIDUAL STRESS FIELDS

Metallic bars are subjected to large plastic deformations during the cold-drawing process. After drawing, strains tend to recover, but they are prevented by previous plastic deformations in some regions inside the material. Such a constraint generates a field of residual strains, and therefore a residual stress distribution arises [6]. It has been found out, both through numerical simulations and experimental tests [6, 12-14], that the cold-drawing process generates an axisymmetrical profile of longitudinal residual stresses.

In order to numerically assess the cold-drawing residual stress distribution in the notched bar being examined, the experimental data reported in Ref. [6] have been used. Such data are related to smooth steel bars manufactured by a cold-drawing process, which produces a 20% reduction of area. Since residual stresses due to cold-drawing may be detrimental as regards mechanical and fatigue properties, two procedures are considered in order to decrease such stresses [6]: (1) a treatment consisting on further drawing with a very small area reduction (about 1%); (2) a treatment based on a combination of heating (at 400°C) and stretching of the bar.

In more detail, smooth round bars with a radius equal to R_0 (with $R_0 = D_0 / 2$) are modelled employing two-dimensional axisymmetrical finite elements, and pre-stresses equal to the above experimental residual stress distributions [6] are assigned to such finite elements. By removing the material in the notched zone (equalling to zero both the elastic modulus and the pre-stress for each finite element in the notched zone), the dimensionless residual stress profiles for notched bars are determined in correspondence to the reduced cross-section S-S (Fig. 1).

The residual stress data numerically obtained are interpolated by best fitting polynomials (i.e. by power series), which are reported in Fig. 3, where the radial coordinate r is normalized with respect to the bar radius R (i.e. $r^* = r / R$, with $R = D / 2$) and the residual stresses $\sigma_{I(res)}(r)$ are normalized with respect to the absolute value $\sigma_{I(res)}(0)$ of the "as drawn" residual stress distribution at the bar centre (Fig. 3). Such polynomials can be expressed by the following equation:

$$\sigma^*_{I(res)}(r^*) \cong \sum_{i=0}^{n} B^*_{i(res)} \cdot (r^*)^i \qquad (1)$$

where:

$$B^*_{i(res)} = \frac{1}{i!}\left(\frac{d^{(i)}\sigma^*_{I(res)}(r^*)}{dr^{*(i)}} \right)_{r^*=0} \tag{2}$$

The coefficients for the three residual stress distributions being analysed are reported in Table 1.

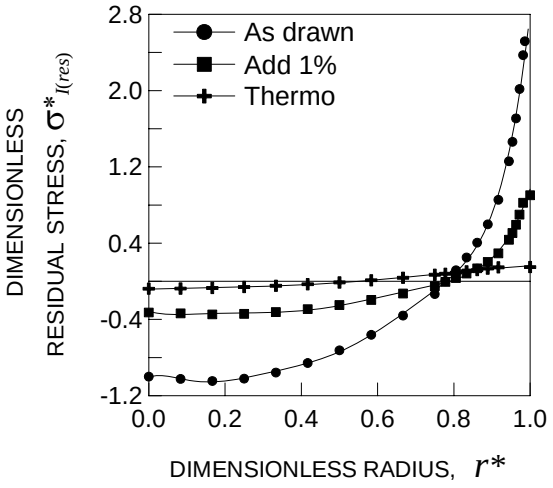

Figure 3: Profiles of longitudinal residual stresses due to mechanical or thermic processes.

Table 1: Polynomial coefficients $B^*_{i(res)}$ of the power series expansions of the dimensionless residual stress distributions $\sigma^*_{I(res)}(r^*)$, reported in Fig. 3.

	$B^*_{i(res)}$								
	0	**1**	**2**	**3**	**4**	**5**	**6**	**7**	**8**
As drawn	-1.01	1.58	-40.05	304.72	-1078.98	2058.77	-2125.54	1091.14	-207.80
Add 1%	-0.32	-1.07	12.14	-57.44	130.73	-136.44	53.37	-	-
Thermo	-0.08	0.13	-0.40	1.12	-0.61	-	-	-	-

4 SIF EVALUATION

In order to evaluate the SIFs produced by the residual stress distributions reported above, the SIFs ($K_{I(i)}$) related to elementary stress distributions ($\sigma_{I(i)} = (r^*)^i$, $i = 0,...,8$) acting on the crack faces are computed along the crack front and properly combined [15-17]. Such SIFs $K_{I(i)}$ are evaluated by means of the quarter-point finite element nodal displacement correlation technique. In a dimensionless form, they can be written as $K^*_{I(i)} = K_{I(i)} / (\sigma_{ref(i)} \sqrt{\pi \cdot a})$, where

$\sigma_{ref(i)}$ represents the reference stress, which is assumed to be equal to the unity for the i-th elementary stress distribution.
Since the superposition principle holds, the dimensionless SIFs corresponding to the residual stresses being analysed can be approximated as [15-17]:

$$K^*_{I(res)} \cong \sum_{i=0}^{n} \sigma_{ref(i)} \cdot B^*_{i(res)} \, K^*_{I(i)} \tag{3}$$

Figure 4 shows the dimensionless SIF $K^*_{I(res)}$ values at points A ($\zeta^* = 1.0$), J ($\zeta^* = 0.5$) and C ($\zeta^* = 0.1$) on the crack front (Fig. 2), for the three residual stress distributions being analysed. Such SIF values are plotted against the relative crack depth ξ ($0.1 \le \xi \le 0.5$), for a semi-circular sickle crack ($\alpha = -1.0$), a straight-fronted crack ($\alpha = 0.0$) and a semi-circular almond crack ($\alpha = 1.0$).

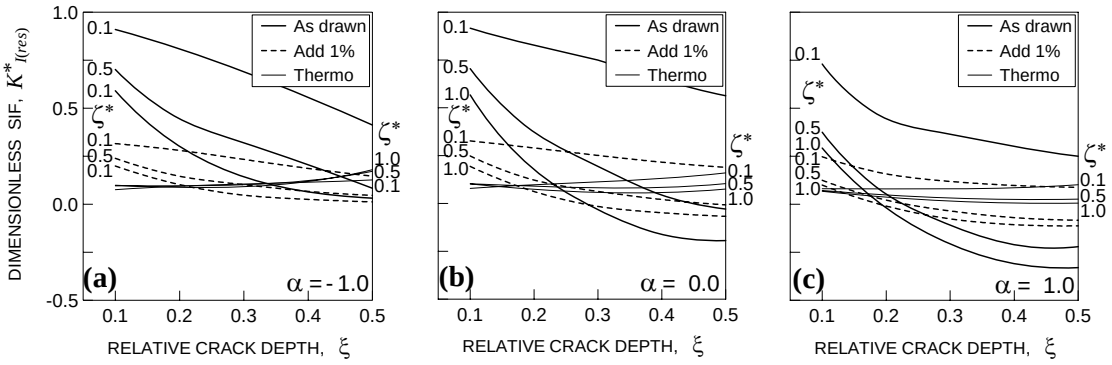

Figure 4: Dimensionless stress-intensity factor $K^*_{I(res)}$ against relative crack depth ξ, for the three residual stress profiles reported in Fig. 3 and for different values of the crack aspect ratio: (a) $\alpha = -1.0$; (b) $\alpha = 0.0$; (c) $\alpha = 1.0$.

For all the considered values of crack aspect ratio α, it can be observed that $K^*_{I(res)}$ decreases by increasing the relative crack depth ξ in the case of both "as drawn" and "add 1%" residual stress distributions, while the SIF increases just a little by increasing ξ in the case of the "thermo" residual stress distribution.

In order to evaluate the SIF produced by tension loading (since the bar is subjected to pulsating tension), a three-dimensional finite element model is adopted. Due to the symmetry, only a quarter of the bar is analysed by employing 20-node isoparametric finite elements. Quarter-point wedge finite elements are used around the crack front in order to model the stress field singularity. A total number of 3186 finite elements and 14357 nodes are employed. Dimensionless SIFs for tension, normalised by means of the reference stress $\sigma_{ref(F)}$, are defined as follows:

$$K^*_{I(F)} = K_{I(F)} / \sigma_{ref(F)} \sqrt{\pi a} \tag{4}$$

where:

$K_{I,F}$ is the SIF for tension F, and $\sigma_{ref(F)} = 8F/\pi D^2$ is the nominal axial stress [18, 19].

In Fig. 5, the dimensionless SIFs $K^*_{I(F)}$ at point A ($\zeta^* = 1.0$), point J ($\zeta^* = 0.5$) and point C ($\zeta^* = 0.1$) on the crack front (Fig. 2) are plotted against the relative crack depth ξ ($0.1 \le \xi \le 0.5$), for a semi-circular sickle crack ($\alpha = -1.0$), a straight-fronted crack ($\alpha = 0.0$) and a semi-circular almond crack ($\alpha = 1.0$).

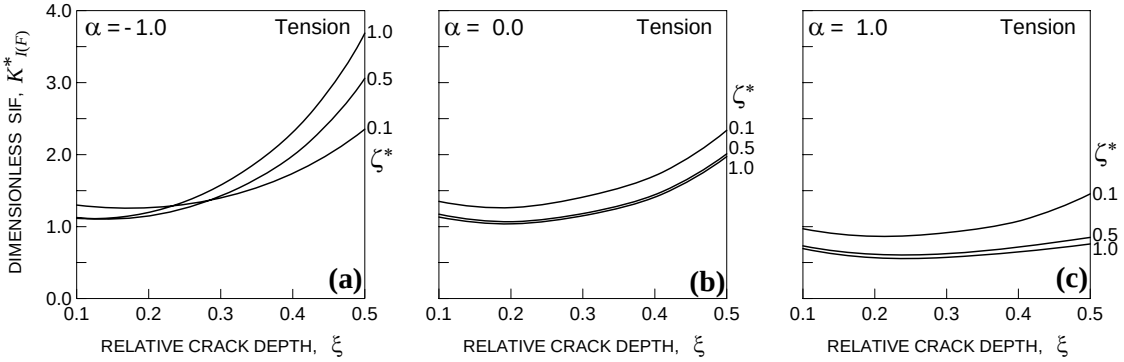

Figure 5: Dimensionless stress-intensity factor $K^*_{I(F)}$ against relative crack depth ξ, for different values of the crack aspect ratio: (a) $\alpha = -1.0$; (b) $\alpha = 0.0$; (c) $\alpha = 1.0$.

5 STRESS RATIO INCLUDING RESIDUAL STRESSES

Since the present paper aims at investigating the effect of the residual stress distributions on the fatigue behaviour of round bars under constant amplitude cyclic tension, the actual stress ratio R_a, which is different from the "nominal" stress ratio $R_F = \sigma_{(F)\min}/\sigma_{(F)\max}$ due to cyclic tension only (where $\sigma_{(F)\min}$ and $\sigma_{(F)\max}$ are the minimum and the maximum tensile stress in a loading cycle), needs to be evaluated also including residual stresses:

$$R_a(r) = \frac{\sigma_{(F)\min} + \sigma_{I(res)}(r)}{\sigma_{(F)\max} + \sigma_{I(res)}(r)} \tag{5}$$

By defining the residual stress severity $s = \sigma_{I(res)}(0)/\sigma_{ref(F)}$ with $\sigma_{ref(F)}$ equal to the maximum stress $\sigma_{(F)\max}$, the actual stress ratio can be written as follows:

$$R_a(r) = \frac{R_F + s \cdot \sigma^*_{I(res)}(r)}{1 + s \cdot \sigma^*_{I(res)}(r)} \tag{6}$$

In Fig. 6, the actual stress ratio R_a is plotted against the dimensionless radial coordinate r^*, for the three residual stress distributions previously introduced and assuming $R_F = 0.0$. It can be

noted that, by increasing the parameter s, the actual stress ratio R_a increases in the outside part of the bar and decreases in the inner part of the bar.

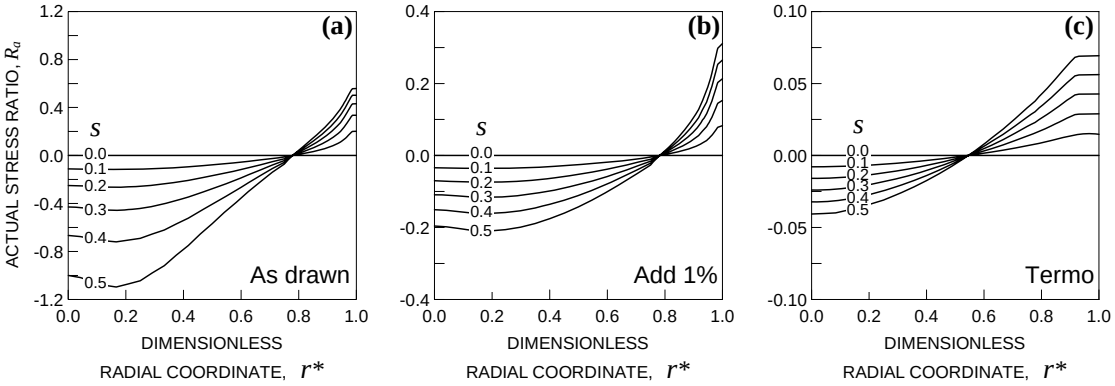

Figure 6: Actual stress ratio R_a against radial coordinate r^*, for different values of s and for three residual stress distributions: (a) as drawn; (b) add 1%; (c) thermo.

6 FATIGUE CRACK PROPAGATION

In order to analyse the fatigue crack propagation under pulsating tension loading, the two-parameter theoretical model proposed in Refs [18, 19] is here applied, by also employing the Paris-Erdogan law [10] modified by means of the Walker relationship [11].

As a matter of fact, it has experimentally been observed [20,21] that the coefficient C of the Paris-Erdogan equation is not only dependent on the material, but also on the stress ratio of the applied cyclic loading. Many equations have been proposed to take into account the stress ratio effect [11, 22-23]. The empirical Walker equation modifies the Paris-Erdogan law as follows [10, 11]:

$$da/dN = \overline{C}(R_a) \cdot \left[\Delta K_I\right]^m \tag{7}$$

where da/dN is the crack growth rate, ΔK_I is the stress-intensity factor range in a loading cycle, and $\overline{C}(R_a)$ is the effective Paris-Erdogan coefficient for the generic stress ratio R_a. Such a coefficient can be expressed by:

$$\overline{C}(R_a) = C_0 \left(1 - R_a\right)^{-(1-\beta)m} \tag{8}$$

where C_0 is $\overline{C}(R_a)$ for $R_a = 0.0$ and β is the Walker exponent. For the problem being examined, ΔK_I in the Eq. (7) is replaced with $\Delta K_{I(F+res)} = \Delta K_{I(F)} = (1 - R_F) \cdot K_{I(F)}$; the parameters C_0 and m are here assumed to be equal to $1.64 \cdot 10^{-10}$ and 2 (with da/dN expressed in [mm·cycle^{-1}] and $\Delta K_{I(F+res)}$ expressed in [N·mm$^{-3/2}$]) [24], and the Walker exponent β is equal to 0.5. Such a fatigue crack growth equation is applied at point A ($\zeta^* = 1.0$) and point C ($\zeta^* = 0.1$) on the crack front, which is assumed to be an elliptical arc during the whole fatigue

crack growth [18, 19]. The cycle number of each fatigue calculation step is taken as a constant and equal to 250 loading cycles.

The diagrams of crack aspect ratio α against relative crack depth ξ are determined for three initial crack configurations, $\sigma_{(F)\max}$ = 100 MPa, R_F = 0.0, and by varying the values of the three residual stress distributions previously introduced (i.e. by varying the parameter s). The crack propagation curves present lower values of α for a given value of ξ by increasing the residual stress severity s.

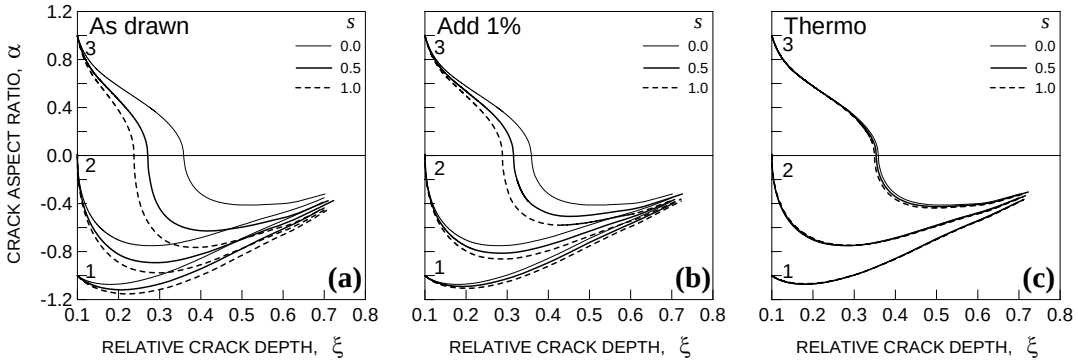

Figure 7: Crack aspect ratio α against relative crack depth ξ, for different values of s and for three residual stress distributions: (a) as drawn; (b) add 1%; (c) thermo.

The crack depth evolution against the number of loading cycles is plotted in Fig. 8 for the three initial crack configurations and the residual stress distributions previously analysed. It can be remarked that the surface crack grows more rapidly in the case of high values of the residual stress severity s.

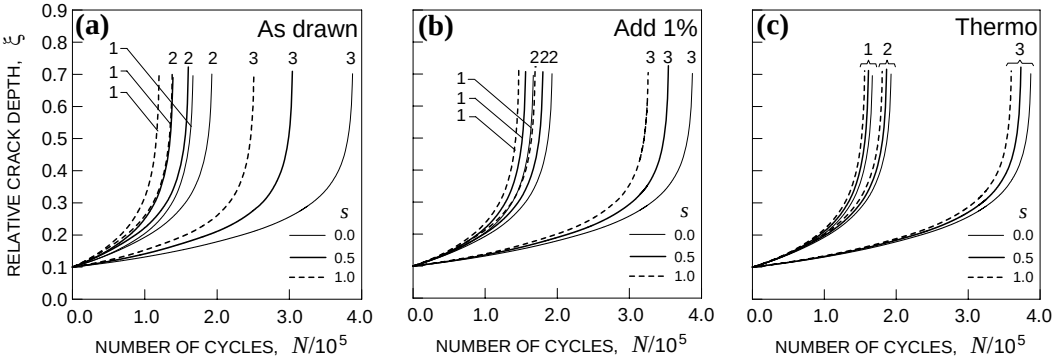

Figure 8: Relative crack depth ξ against number N of loading cycles, for different values of s and three residual stress distributions: (a) as drawn; (b) add 1%; (c) thermo.

7 CONCLUSIONS

In the present paper, the effect of residual stresses due to cold-drawing process and post-drawing treatments (mechanical and thermo-mechanical) on the fatigue behaviour of a metallic notched round bar with a surface crack has been examined. Different values of the residual stress distributions have been considered, and the bar has been assumed to be also subjected to cyclic tension. The fatigue crack propagation has been analysed by using the Paris-Erdogan law modified by the Walker equation, in order to take into account the effect of the actual stress ratio.
It has been observed that the residual stress field appreciably influences both the crack aspect ratio evolution and the crack growth rate. In particular, the surface crack grows more rapidly in the case of high values of the residual stress severity s. Because of the detrimental effect of residual stresses due to standard cold-drawing on fatigue, surface treatments are advised in order to relieve residual stresses after drawing.

References

[1] Shijve, J., *Fatigue of Structures and Materials*, Kluwer Academic Publishers, New York (2004).

[2] Caspers M., Mattheck C. and Munz D., "Propagation of surface cracks in notched and unnotched rods. Surface-crack growth: models, experiments and structure", *ASTM STP*, **1060**, 365–389 (1990).

[3] Lin X.B. and Smith R.A., "Fatigue growth simulation for cracks in notched and unnotched round bars", *International Journal of Mechanical Sciences*, **40**, 405–419 (1998).

[4] Lin X.B. and Smith R.A., "Shape evolution of surface cracks in fatigued round bars with a semicircular circumferential notch", *International Journal of Fatigue*, **21**, 965–973 (1999).

[5] Carpinteri A., Brighenti R. and Vantadori S., "Surface cracks in notched round bars under cyclic tension and bending", *International Journal of Fatigue*, **28**, 251–260 (2006).

[6] Elices M., "Influence of residual stresses in the performance of cold-draw pearlitic wires", *Journal of Materials Science*, **39**, 3889–3899 (2004).

[7] Gardin, S., Courtin S., Bèzine G., Bertheau D. and Ben Hadj Hamouda H., "Numerical simulation of fatigue crack propagation in compressive residual stress fields of notched round bars", *Fatigue & Fracture of Engineering Materials & Structures*, **30**, 231–242 (2007).

[8] Gardin, S., Courtin S., Bèzine G., Bertheau D. and Ben Hadj Hamouda H., "The influence of roller burnishing on the fatigue crack propagation in notched round bars - Experimental observations under three-point bending", *Fatigue & Fracture of Engineering Materials & Structures*, **30**, 342–350 (2007).

[9] Fuchs H.O. and Stephens R.I. (Eds.), "*Metal fatigue in engineering*", John Wiley and Sons, New York (1980).

[10] Paris P.C. and Erdogan F.J., "A critical analysis of crack propagation laws", *Journal of Basic Engineering*, **85**, 528–534 (1963).

[11] Walker K., "The effect of stress ratio during crack propagation and fatigue for 2024-T3 and 7075-T6 aluminium", *ASTM STP*, **462**, 1-14 (1970).

[12] Macherauch E. and Kloos K.H., "Origin, measurements, and evaluation of residual stress in science and technology", in: *Proceedings of International Conference on Residual Stresses* Garmisch-Partenkirchen, Germany, 3-26, (1986)

[13] Kalpakjian S. (Ed.), "*Manufacturing processes for engineering materials*", Adison-Wesley Publishing Company, 1991.

[14] Atienza J.M. and Elices M., "*Influence of residual stresses in the relaxation of cold drawn wires*", Materials and Structures, **37**, 301-304, (2004).

[15] Carpinteri A., Brighenti R. and Vantadori S., “Circumferentially notched pipe with an external surface crack under complex loading”, *International Journal of Mechanical Sciences*, **45**, 1929–1947 (2003).
[16] Carpinteri A., Brighenti R. and Vantadori S., “Notched shells with surface cracks under complex loading”, *International Journal of Mechanical Sciences*, **48**, 638–649, (2006).
[17] Carpinteri A., Brighenti R., Vantadori S. and Viappiani D., “Sickle-shaped crack in a round bar under complex Mode I loading”, *Fatigue & Fracture of Engineering Materials & Structures*, **30**, 524–534 (2007).
[18] Carpinteri A., “Shape change of surface cracks in round bars under cyclic axial loading”, *International Journal of Fatigue*, **15**, 21–26 (1993).
[19] Carpinteri A. and Vantadori S. , “Sickle-shaped surface crack in a notched round bar under cyclic tension and bending”, *Fatigue & Fracture of Engineering Materials & Structures*, **32**, 223–232 (2009).
[20] Maddox S.J., “The effect of mean stress on fatigue crack propagation”, *International Journal of Fracture*, **11**, 389–408 (1975).
[21] Iost A., “The effect of load ratio on the m-lnC relationship”, *International Journal of Fatigue*, **13**, 25–33 (1991).
[22] Ibrahim F.K., “The effect of stress ratio, compressive peak stress and maximum stress level on fatigue behaviour of 2024-T3 aluminium alloy”, *Fatigue & Fracture of Engineering Materials & Structures*, **12**, 9–18 (1989).
[23] Zheng J. and Powell B.E., “Effect of stress ratio and test methods on fatigue crack growth rate for nickel based superalloy Udimet720”, *International Journal of Fatigue*, **21**, 507–513 (1999).
[24] Gurney T.R., “*Fatigue of Welded Structures*”, Cambridge University Press, Cambridge (1979).